2014 IEEE International Conference on Robotics & Automation (ICRA)
Hong Kong Convention and Exhibition Center
May 31 - June 7, 2014. Hong Kong, China

RoboRay Hand : A Highly Backdrivable Robotic Hand with Sensorless Contact Force Measurements

Yong-Jae Kim, Younbaek Lee, Jiyoung Kim, Ja-Woo Lee, Kang-Min Park,
Kyung-Sik Roh and Jung-Yun Choi

Abstract— **This paper presents a 14-DOF robotic hand including 5 fingers and a wrist. The hand has a new tendon-driven mechanism which minimizes frictional loss and maximizes efficiency and backdrivability. In order to accomplish high efficiency and backdrivability as well as human-like payload and dexterity in a compact size, two novel mechanical concepts are proposed. Firstly, the actuators are placed according to the functions of fingers – high power grasping and precise manipulation - instead of positioning at each joint. For the high power grasping, 7 high payload motors are positioned in the forearm, and 5 small size motors are positioned in the palm for the precise manipulation. Secondly, a new tension decoupling mechanism is proposed to the 2-DOF wrist joint, which delivers wire motions of the forearm motors to the fingers without frictional loss or coupling with wrist motion. A total weight including the forearm is 1.59kg which is similar to human. The fingertip force is 15N which is sufficient for most of household work. High backdrivability enables the contact force sensing by measuring a motor current without additional sensors. A detectable minimum contact force was 0.735N. In order to enhance the contact force sensing capability, a friction compensation algorithm was applied, which resulted to the minimum contact force as 0.196N. Theoretical and experimental analyses are also performed.**

I. Introduction

HUMAN hands are one of the most versatile tools of organic devices. They can not only exert high forces when compliantly grasping various objects, but can also precisely manipulate small objects. Robotic hands have been evolved in order to mimic these two characteristics.

Research on robotic hands can be roughly categorized into two groups: the dexterous robot hands with high degrees of freedom (DOF) and the compliant robot hands with an underactuated mechanism or flexible material. A high DOF dexterous robot hands have been developed over several decades, e.g. the MIT/Utah hand [1], Robonaut Hand by NASA [2], DLR hand [3], Dexterous Hand by Shadow Co., GIFU hand [4] and AIST hand [5]. These hands have from 12 DOF to18 DOF and have the same number of actuators. Due to a large number of actuators, they are prone to have substantial size and weight or relatively low payload .

Manuscript received Sept. 15, 2013. This work was supported in part by SAIT of Samsung Electronics.

Y.J Kim, J. Kim, J.W. Lee, K.M. Park, K.S. Roh and J.Y Choi are with Samsung Advanced Institute of Technology, Ki-hung gu, Yong-in si., Kyunggi do, Rep. of Korea. (corresponding author to provide phone: +82-31-280-1529, e-mail: yj424.kim@samsung.com)

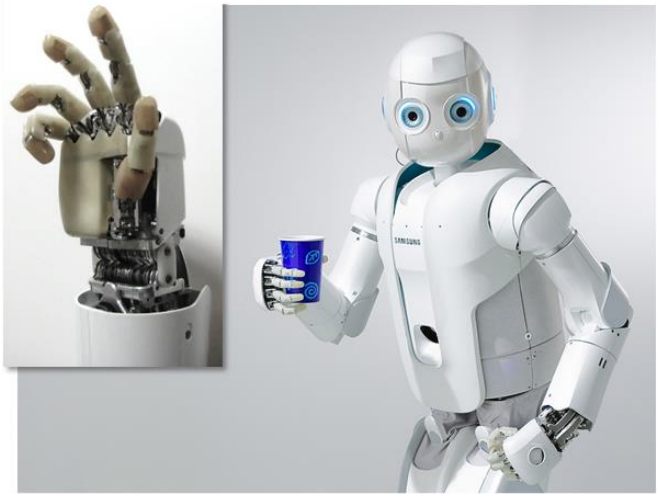

Fig. 1. RoboRay, a humanoid robot with two life-size dexterous robotic hands developed in Mechatronics Center of Samsung Electronics [9][10].

Small motors with high reduction gears can increase the payload, but the hand loses backdrivability and speed. Placing large size and high torque motors in the forearm has been frequently tried to reduce the size of hands. Wires and conduits are commonly used for the cable tension transmission from the forearm to the fingers, and torsion cables for transferring rotational motion as well [2]. These are simple and effective approaches to decouple the finger motion from the wrist. However, they can restrict the wrist range of motion and increase the frictional loss.

The other category is on compliant robot hands with underactuated mechanisms [6]. The mechanical compliance enables grasping of various objects without complicated control with a large number of actuators. Moreover, payload can be easily increased by using a small number of high torque actuators. Recently, due to these advantages, the underactauted mechanism has been widely applied to the robot hands such as prosthetic hands or graspers for exploring field [7,8]. However, the downside is that precise manipulation is inherently difficult.

Our goal is to develop a life-size robotic hand having both of the precise manipulability and the compliant power grasping capability. Our main reason developing human like robotic hands is for robots to share human tools and environment. From this point of view, we do not have to mimic the human hand anatomy. Instead, we adopt the advantages of human hands such as a size, shape, weight, and even payloads in the functional level. The developed robotic hand, named RoboRay hand, has 5 fingers with 12 DOF and a

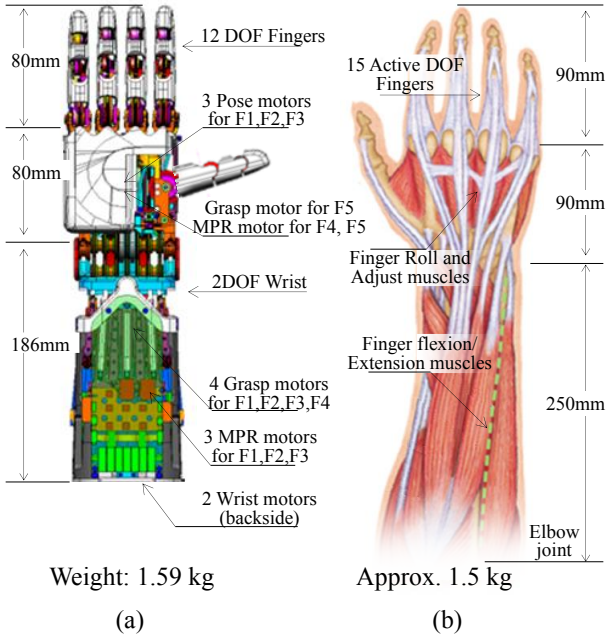

Fig.2. Size and shape comparison, (a) RoboRay hand, (b) human hand and forearm with average size and proportion of adult males.

wrist with 2 DOF. The new tendon driven mechanism minimizes frictional loss and increases efficiency and backdrivability. Linear actuators composed of motors and ball screws actuate fingers via wires and pulleys. In order to accomplish high efficiency and backdrivability, two novel mechanical concepts are applied. Firstly, the actuators are deployed according to the function of the finger instead of the joints. The grasping functions of the hand can be divided into power grasping by using whole hand and precision handling by using fingertips [11]. For the power grasping, 7 large-size motors are positioned in the wrist, and, for the precision handling, 5 small size motors are deployed in the palm. Secondly, a new 2-DOF tendon transmission mechanism is applied for the wrist joint, which facilitates tension transmission with low frictional loss and eliminates coupling between wrist motion and wire for the fingers. These high efficiency and backdrivability enables contact force sensing over whole contact points of fingers, while many other robotic hands rely on expensive force sensors.

This paper is organized as follows: the design concepts are introduced in Section II. Section III describes the mechanical design in detail. In Section VI, a friction compensation algorithm was proposed in order to enhance the contact force sensing capability. The mechanical properties and the capabilities are investigated by the system analysis and experiments in Section V. Section VI concludes this paper.

II. DESIGN CONCEPTS

Fig.2 compares the size and shape of the developed robotic hand and the average adult male's hand, where F1, F2, F3, F4 and F5 denote the thumb, index finger, middle finger, ring finger and little finger, respectively. For 3-dimensional dexterous manipulation, 3-DOF for each of F1, F2 and F3 is indispensable, thus the hand was designed to have 3 DOFs for

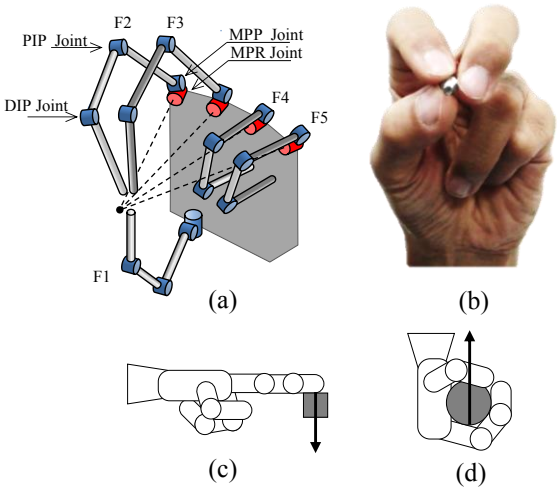

Fig.3. Requirements of life-like robotic hands, (a) a kinematic structure of the RoboRay Hand, (b) a human hand in 3-fingered precision handling, (c) fingertip force measurement, (d) power lift measurement.

F1, F2 and F3. As shown in Fig.3(a), each finger of these has 3 joints, named DIP, PIP, and MP joints. The DIP and PIP joint are coupled to flex together to have 1 DOF like human joints, and the 2-DOF MP joint is considered as 2 separated joints, named as MPP (MP pitch for flexion motion) and MPR (MP roll for abduction/adduction motion) joints. F4 and F5 have totally 3-DOF for underactuated grasping and adduction/ abduction motion. The size of the fingers and the palm was chosen similar to the humans, and the forearm is compact enough to be mounted on a robotic arm. The following describes the design concepts of the RoboRay hand:

- Bio-mimetic mechanism based on functionality

In order to adopt the advantages of the human hand without just mimicking the anatomy, we focused on the purpose and functionality of the human hand feature. A noteworthy feature of the human hand is that the large muscles for fingers are placed in the forearm as shown in Fig.2(b). The forearm is a useful place for both of the robotic hand and human hand to generate high force of fingers. In order not to sacrifice the efficiency and range of motion of the wrist while using forearm portion, we came up with a wrist mechanism different from humans, named 2-DOF tension decoupling mechanism, which will be explained in detail in Section III.A.

Another feature worthwhile to consider is opposition between the thumb and other fingers. The high opposition enables delicate handling by using fingertips. Humans have highest opposability index 60 among primates followed by baboons 57-58 and orangutans 40 [12]. Therefore, we selected the thumb and finger configuration to achieve high opposability index 100 and completely opposing directions as shown in Fig.3(a) and it was verified in Section V.

The other interesting feature of the human hand which can be overlooked is the configuration of MPR joints. Human fingertips can easily become adjacent as shown in Fig.3(b) because the MPR axes intersect the one point as shown in Fig.3(a), which is the key ability for 3 fingered manipulation of small objects. On the other hand, if the MPR axes are

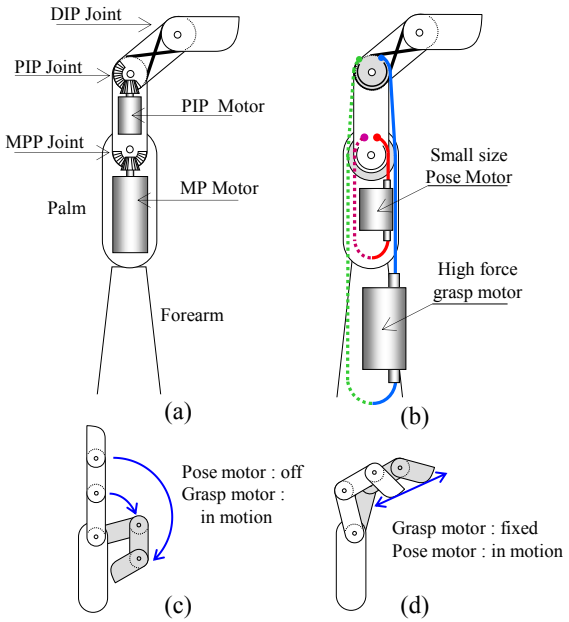

Fig. 4 Actuator configurations, (a) conventional actuator positioning located at each joint, (b) configuration based on the grasping functions, (c) power grasping using forearm motors, (d) precise motion using palm motors.

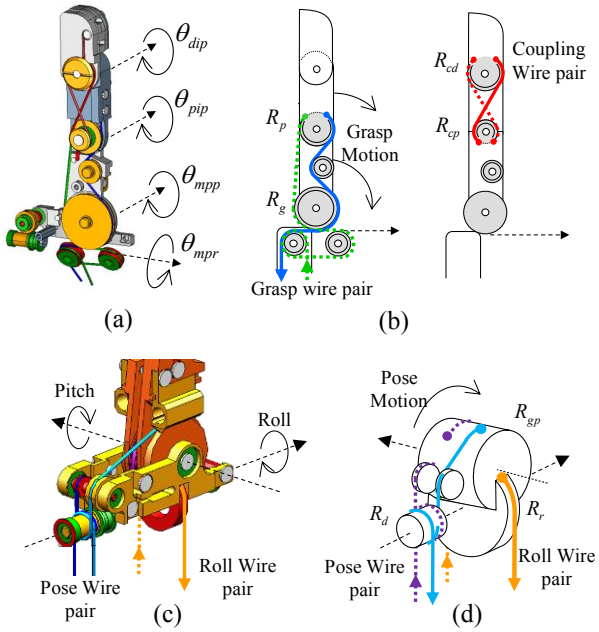

Fig.5 Detailed design of the finger.

parallel to each other, as many robotic hands, the fingertips are difficult to be touched each other near the center of palm. Therefore we designed the MPR direction for the axis to intersect one point as Fig.3(a) and it is verified in Section V.

- Compactness and modularity

Our goal is to use the robotic hands in the same environment for humans. As it must be mounted on a human -sized robotic arm, the compactness and modularity are also important factors. The forearm with 9 high force motors has the volume of 83mm×76mm×186mm, which is sufficiently compact to attach to a robotic arm with an elbow joint and a forearm rotation joint. The forearm includes the motor drivers and controllers, and the only electric connections are for the power and communication.

For agile manipulation like humans, the robotic hand should be light-weight and the mass center is better to locate as close to the proximal position as human's hands and forearms. The implemented hand has 1.59kg which is similar to the human's weight 1.5kg and the mass center is one third of the total height.

- Payload and Speed

The fingertip force in a stretched pose as shown in Fig. 3(c) is one of the representative criterion of the robotic hand. Average adult can exert the peak fingertip force of about 40N. After investigating the conventional household works, we decided that more than 40N lifting force and 10N fingertip force are required.

In addition to the payload, high speed is also crucial requirement for human like hand motion. The maximum finger joint speed is greater than 500deg/sec which is challenging for the mechanisms composed of small motors with high reduction gears. Therefore, in order to achieve the high payload and high speed, we utilized a forearm portion for high force motors with low reduction ratio and minimized the frictional loss throughout the transmission mechanisms.

- Backdrivability

Backdrivability implies more than energy conservation. The robotic hands with high reduction ratio have low backdrivability caused by the friction and damping of reduction gears. Thus, it is difficult to apply force control without force torque sensors or tactile sensors. Instead, they tend to utilize admittance control with aid of expensive force sensors or relatively unreliable tactile sensors. However, these approaches can restrict system bandwidth and it is difficult to deal with the contact on the hand surface where the sensors do not cover. In order to realize compliant manipulability like humans, backdrivability is essential.

III. Mechanical Design

A. Actuator Configuration Based on the grasping functions

Fig.4(a) illustrates the concept of conventional robotic fingers. For the convenience of explanation, it was simplified to 2-dimensional model where MPR joint was omitted. The motors are connected directly to the MP joint and the PIP joint, which simplifies the mechanism, but the motor payload is limited due to the size. Especially, the small PIP motor in the finger frame severely hinders increasing the fingertip force.

In order to overcome this problem, we propose a modified concept of the underactuated hands. As shown in Fig.4(b), the wire pair (blue and green line) from the high force motor is connected to PIP joint passing through a free rotating pulley on MPP joint, and the wire pair (red and purple line) from the small-size motor is connected to the MPP joint. If the small-size motor is turned off and the high force motor works, the fingers perform grasping motion as an underactuated hand as shown in Fig.4(c). On the other hand, if the high force motor is fixed and the small motor works, the pose of the

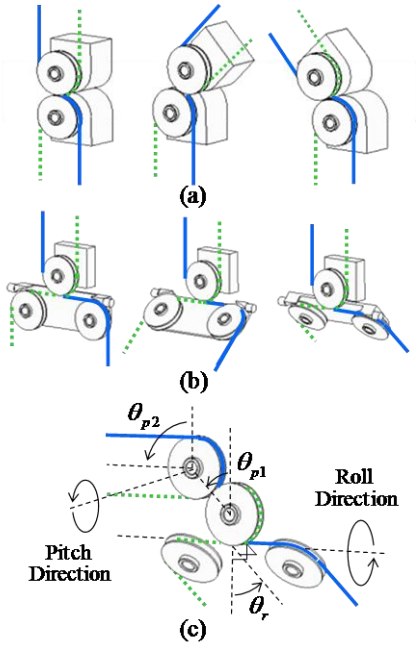

Fig. 6 Tendon decoupling mechanism

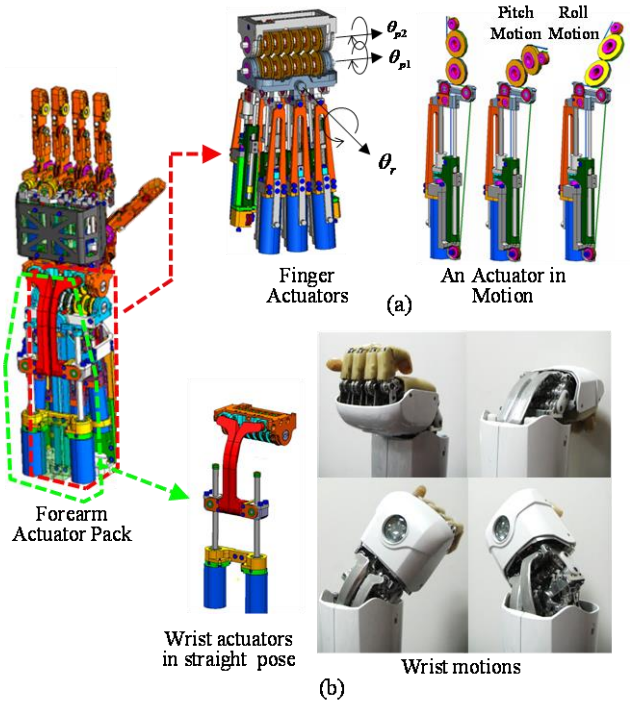

Fig. 7 Detailed design of the wrist

fingertip can be adjusted precisely as shown in Fig4.(d). Thus, considering the function of each motor, the high force motor and the small motor are named as grasp motor and pose motor, respectively.

By mounting the pose motors and grasp motors properly in the palm and forearm (refer to Fig.2(a)), we can achieve a human-sized hand mechanism which has the high force grasping capability as well as precise manipulation capability.

Fig.5 shows the detailed design of the 3-DOF finger, which is actuated by the 3 wire pairs named grasp, pose and roll wire pairs and 1 wire pair for PIP and DIP joint coupling. In order to minimize friction, pulleys with bearings are used for the overall path of the wires. The mechanism of the grasp wire pair and the pose wire pair is conceptually the same as in Fig.4(b). However, the connection of the grasp and pose wire pair through the MPR joint is difficult to implement.

Fig.4(a) and (b) illustrate the detail design and its conceptual diagram of the grasp and coupling wire pairs. The grasp wires pass through the MPR axis before connected to the actuator side. Thus the MPR motion does not affect the length of the grasp wires, instead they are slightly twisted. For the coupling between the DIP and PIP joints, a 8-shaped wire is used as shown in Fig.4(b). Fig.4(c) and (d) illustrate the detailed design and the conceptual diagram of the pose and roll wire pairs. As MPR axis center is already occupied by the grasp wires, an additional redirection pulley is used for the connection. As shown in Fig.5(d), the roll wire pairs actuate the MPR joint, whose actuator is also placed at the forearm portion.

The three wire pairs are actuated by three linear actuators composed of ball screws and electric motors. If we denote the rotating angle of the roll, pose and grasp motors as ϕ_{roll}, ϕ_{pose} and ϕ_{grasp}, respectively, and the resultant rotating angle of the DIP, PIP, MPP and MPR joints as $\theta_{dip}, \theta_{pip}, \theta_{mpp}$ and θ_{mpr}, respectively, the relationship between the motor rotation and the joint motion can be derived as follows:

$$\begin{bmatrix} \theta_{mpr} \\ \theta_{mpp} \\ \theta_{pip} \\ \theta_{dip} \end{bmatrix} = \begin{bmatrix} \frac{G_r}{R_r} & 0 & 0 \\ \frac{G_r R_d}{R_{gp} R_r} & \frac{G_p}{R_p} & 0 \\ -\frac{R_d G_r R_g}{R_p R_r R_{gp}} & \frac{G_p R_g}{R_p R_{gp}} & \frac{G_g}{R_{gp}} \\ -\frac{R_d G_r R_g R_{cp}}{R_p R_r R_{gp} R_{cd}} & \frac{G_p R_g R_{cp}}{R_p R_{gp} R_{cd}} & \frac{G_g R_{cp}}{R_{gp} R_{cd}} \end{bmatrix} \begin{bmatrix} \phi_{roll} \\ \phi_{pose} \\ \phi_{grasp} \end{bmatrix} \quad (1)$$

where G_r, G_p and G_g denote the reduction ratio from the rotations of roll, pose, and grasp motors to the linear motions of corresponding ball screws. R_p and R_g mean the diameters of pulleys comprising grasp wire path as shown in Fig.5(b), and R_{gp} and R_d denote the diameters of pulleys comprising pose wire path as shown in Fig.5(d). R_{cd}, R_{cp} and R_r denote the pulleys for coupling wires in Fig.5(b) and the pulley for MPR motion in Fig.5(d).

B. 2-DOF Tension decoupling mechanism for the wrist

The proposed finger mechanism has high efficiency due to low frictional loss. However, the overall system can have low efficiency if the friction between the fingers and the actuators in the forearm and wrist is substantial. Moreover, wire connections between the fingers and the actuators are possible to limit the ranges of motion for the 2-DOF wrist.

In order to minimize friction and maintain a human-like range of motion, we propose a new efficient and compact tension transmitting mechanism for the wrist. Fig. 6(a) shows a basic concept of a tension decoupling mechanism using a

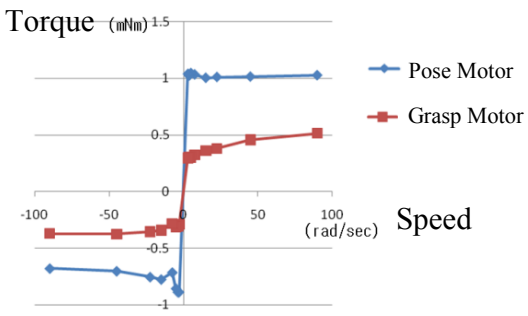

Fig. 8 Friction-speed graph for a grasp motor and a pose motor

rolling joint, where the joint is composed of two links with a cylindrical surface which has rolling contact and two freely rotating pulleys placed at the center of each cylindrical surface. The solid wire and dotted wire mean agonistic tendon and antagonistic tendon, respectively. Due to the rolling motion, the length of the two wires does not affect the motion of the joint.

Another basic concept of tension decoupling mechanism uses an offset pivot, as shown in Fig. 6(b). The grooves of the three pulleys in this figure are on the pivot axis, and the wire going through these pulleys is collinear to the pivot axis. Therefore, the rotation of the pivot also does not affect the length of the wires. While rotating, the wires are slightly twisted. From repeated experiments, we obtained the safe range of motion for our system – approximately ±60°.

By combining these two mechanisms, 2-DOF tension decoupling mechanisms was devised as shown in Fig.5(c). The rolling contact motion keeps the rotating angles in a fixed ratio: $\theta_{p2} = 2\theta_{p1}$. It satisfies our target range $-90° < \theta_{p2} < 90°$ and $-45° < \theta_r < 45°$ for the wrist as shown in Fig.7(b). Multiple wires can be transmitted by stacking the proposed mechanism in parallel. The tension decoupling mechanism for 7 wire pairs were implemented as shown in Fig.7 (a). Because every actuator has common rotation axes for θ_{p1} and θ_{p2} motions, but a different rotation axis among the others for θ_r motion. Thus, when the wrist is in θ_r motion, some of the 7 actuators do not only rotate, but also translate slightly up and down direction. Therefore, the forearm frame was designed to secure the room with proper guiding structure for the translational motions. The wrist is actuated by two parallel links, balls crews and motors as shown in Fig.7 (b) because the wrist is occupied by the tension decoupling mechanism.

Similar to the finger mechanism, every pulley in the forearm and wrist mechanism has a bearing to minimize friction. Therefore, the implemented hand achieves high efficiency and backdrivability, which enable the sensitive contact force measurement capability by using motor current sensing without expensive force-torque sensors or haptic sensors.

IV. Friction Compensation

In order to further enhance the contact force measuring capability, we propose an online friction compensation algorithm. Fig.8 shows experimental results of the frictional

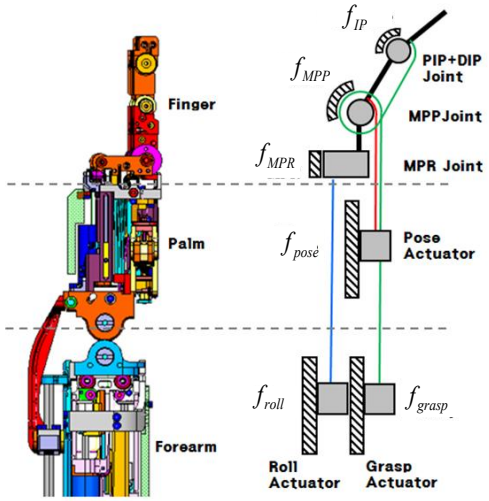

Fig. 9 Diagram of frictions

torque by measuring motor current where the blue curve and red curve denote the result of a grasp motor and a pose motor of F2, respectively. Because there was no external contact or gravitational effect in these experiments, this means the internal frictional loss. From these graphs, we can notice that the Coulomb friction is dominant compared to the stiction or viscous friction, and the amount of the Coulomb friction is not symmetric according to the direction. From repeated friction tests for the actuators, we found that the asymmetry comes from the actuators.

If all the Coulomb friction parameters of the fingers are obtained and compensated, the contact force measuring capability can be improved. Fig.9 shows a schematic drawing describing the friction points of a finger. The frictions of the DIP joint and the PIP joint were merged into a single friction f_{IP} and the frictions of roll actuator and the MPR joint also can be considered as one friction f_{roll} for the convenience.

Therefore, the Coulomb friction parameters to be obtained for each finger are $f_{IP}, f_{MPP}, f_{roll}^{+}, f_{roll}^{-}, f_{pose}^{+}, f_{pose}^{-}, f_{grasp}^{+}$ and f_{grasp}^{-} (totally 8), where f_{IP} and f_{MPP} denote symmetric Coulomb frictions of the joints, and the others mean the asymmetric Coulomb frictions of the actuators in both directions. One hand has 30 parameters because each of F1, F2 and F3 has 8 parameters and F4 and F5 have totally 6 parameters considering 3 actuators for F4 and F5. The main challenge of the compensation is to obtain these many parameters easily and rapidly.

Now let us focus on one of 3-DOF fingers. If we define a matrix $\bar{J}$ as a 3×3 Jacobian matrix from the actuator speed to the joint speed, it has the same elements as (1) except the last raw. Considering the virtual work, the relationship between the actuator torque and the joint torque as follows:

$$\begin{bmatrix} \tau_{roll} \\ \tau_{pose} \\ \tau_{grasp} \end{bmatrix} = \bar{J}^T \left(\begin{bmatrix} \tau_{MPR} \\ \tau_{MPP} \\ \tau_{IP} \end{bmatrix} + \begin{bmatrix} 0 \\ \pm f_{MPP} \\ \pm f_{IP} \end{bmatrix} \right) + \begin{bmatrix} f_{roll}^{\pm} \\ f_{pose}^{\pm} \\ f_{grasp}^{\pm} \end{bmatrix}, \quad (2)$$

where τ_{roll}, τ_{pose}, and τ_{grasp} denote the torques of the roll, pose and grasp actuators, and τ_{MPR}, τ_{MPP}, and τ_{IP} denote the

TABLE I
MOTION SET FOR FRICTION PARAMETER ACQUISITION

Directions					Motions
f_{IP}	f_{MPP}	f_{roll}	f_{pose}	f_{grasp}	
+	+	+	+	+	Grasping with MPR plus rotation
−	−	−	−	−	
+	+	−	+	+	Grasping with MPR minus rotation
−	−	+	−	−	
−	+	+	+	−	MPP flexion and PIP extension
+	−	−	−	+	with MPR plus motion
−	+	−	+	−	MPP flexion and PIP extension
+	−	+	−	+	with MPR minus motion

torque exerted to the MPR, MPP and the sum of PIP and DIP joints. The signs (±) in (2) can be determined according to the rotation directions of joints and actuators. Once 8 parameters are obtained, (2) can be used as a friction compensation algorithm. For a stable compensation, an algorithm for compliant transmission [13] was applied. Hereafter, the parameter identification algorithm is explained.

If the finger moves without external force , τ_{MPR}, τ_{MPP}, and τ_{IP} are all zero and we can obtain 3 equations from (2) based on the measured actuator torques τ_{roll}, τ_{pose}, and τ_{grasp}. As the number of signs in (2) is 5 and in each case, the number of equations is 3, we can get 96 equations (3×2^5) by changing the rotation directions of joints and actuators. However, in actual case, many of these motions are practically infeasible. Thus, representative motions were selected as Table I considering the feasibility and the enough range of motion, where the number of motions is 8 including the corresponding inverse motions. After carrying out these 8 motions, 24 (3equations× 8 motions) equations are obtained and these can be expressed as a matrix form as:

$$T_{act} = J_{motion} F_{param} \tag{3}$$

where T_{act}, J_{motion} and F_{param} denote a vector composed of measured 24 actuator torques (3 actuators× 8 motions), 24×8 matrix form of the equations obtained from (2) and the vector composed of 8 parameters. As the number of equations are more than the number of the unknown parameters and J_{motion} has rank 8, the parameters can be calculated as follows by using pseudo inverse of J_{motion}:

$$F_{param} = (J_{motion}^T J_{motion})^{-1} J_{motion}^T T_{act} \tag{4}$$

Fig.10 (a) shows the experimental setup of the friction test. Due to a load cell with a lever, the actual contact force can be measured with 0.023N sensitivity. After repeated experiments, we obtained that the finger can detect 0.2N reliably while it can detect 0.74N without compensation. Fig.10 (b) shows snapshots of pinching test by using the proposed compensation algorithm. The bottle weighed 230g is placed in arbitrary position and the joint level impedance control was applied for pinching. Without the friction compensation, the hand failed to pinch it because the hand could not detect the contact properly. With the friction compensation, on the other hand, the hand could pinch the bottle without fail.

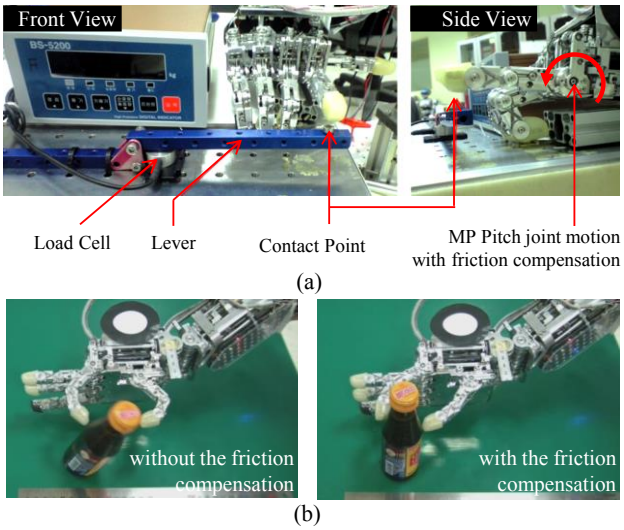

Fig. 10 Experimental setup and the pinching experiment

The proposed compensation algorithm has an advantage that the parameters can be obtained rapidly by performing simple calibration motion as shown in Table I, which requires about 4 seconds. Therefore, even though the parameters have changed due to the change of lubrication condition or wire pretension, the hand can be easily recalibrated just before handling objects.

V. EXPERIMENTAL VALIDATION

Table II summarizes the specification of the RoboRay hand. Please note that the speed of all the joints is sufficiently high enough to perform agile and dexterous hand motions. The relatively low reduction ratio also helps achieving high backdrivability due to minimizing amplifications of the friction, damping and inertia of the motors. Most of the frames were made from aluminum alloy (AL 6061T6) and steel wires which have 7x19 constructions and 0.8mm diameters were used for actuation. The ball screws for the fingers and the wrist have 1 mm lead.

Fig.11 shows several motions of the RoboRay hands. As shown in Fig.11(a)~(d) all fingers have high opposition capability. Fig.11(e) shows the advantage of the proposed MPR configuration that facilitates small object manipulation. Fig11(f) is a snapshots of a dynamic paper cup manipulation, which needs more than 400deg/sec joint speed. Fig.12 shows several snapshots of dual hand-arm motions. The robot demonstrates a manipulation of L-shaped wrench in Fig.12 (a), (b) and (c), where a joint space impedance control was applied for pinching the small object. Fig.12(d),(e) and (f) shows the ball manipulation motion, where an actuator space impedance control was applied for compliant grasping.

VI. CONCLUSION

A highly efficient and backdrivable robotic hand, named RoboRay hand, was introduced. It has 12 DOF for 5 fingers and 2 DOF for the wrist. The human-like size and shape, weight and performance enables handling the objects and tools for human in the human environment. By placing the

TABLE II
SPECIFICATIONS OF THE ROBORAY HAND

Items	Specifications	
Weight	1.59 kg	
Dimensions	Hand (H×L×W)	160 × 80 × 45 mm
	Forearm (H×L×W)	186× 76× 83 mm
DOF	Finger	12 DOF / 5 fingers
	Wrist	2 DOF
Payload	Peak Fingertip force	15N
Speed / Reduction ratio	MPR joint	800deg/sec, 47:1
	MPP joint	700deg/sec, 57:1
	PIP joint	450deg/sec, 82:1
Actuation	Motor, ball screw, wire and pulley	
Sensing	Minimum force sensing without Compensation : 0.735N with Compensation : 0.196N	
Motor	Pose motion	1.8Watt DC motor
	Grasp & roll motion	8Watt BLCD motor
	Roll motion	12Watt BLCD motor
Electronics	DC 12V, DSP TMS320F2812 EtherCAT communication	

actuators according to the grasping functions, it can have the inherent capabilities of compliant high-power grasping and high precision manipulation. In order to placing high payload motors in the forearm without increasing friction and coupling, a unique tendon transmitting wrist mechanism was developed. A total weight including the forearm is 1.59kg similar to human, and the peak fingertip force is 15N which is sufficient for most of household work. High backdrivability enables the contact force sensing by measuring motor current without additional sensors. It can detect the minimum contact force as 0.196N with the proposed online friction compensation algorithm.

For future research, tactile sensors will be tested and applied, and continuous improvements, such as contact shape optimization, durability improvement and water resisting function, will be performed.

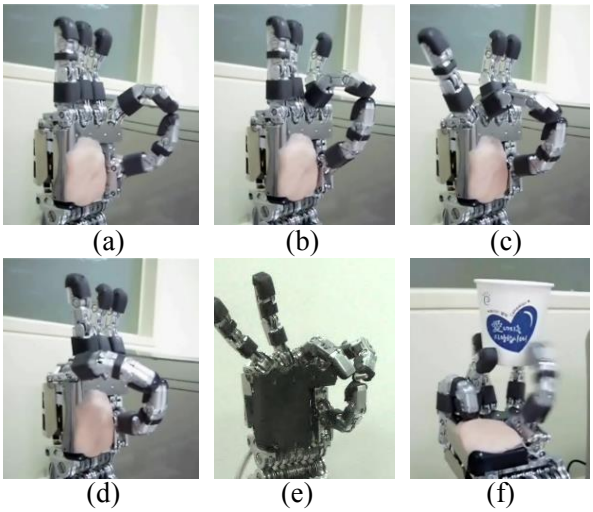

Fig. 11. A developed hand performing basic motions and manipulation.

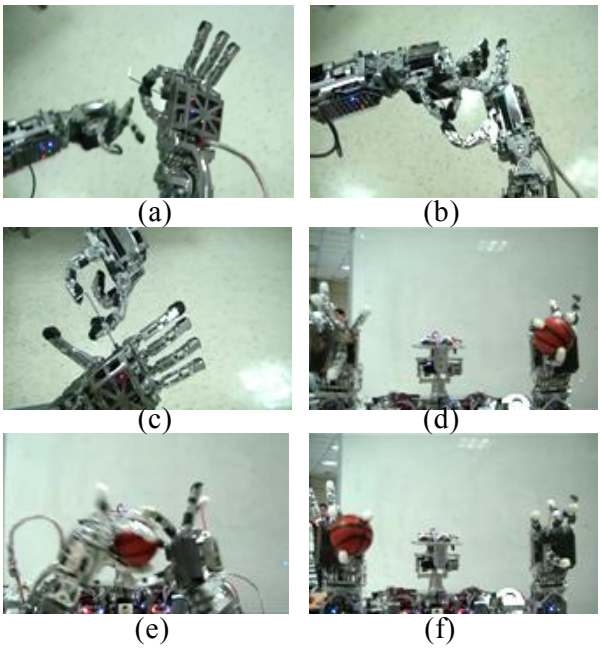

Fig.12. Snapshots of object manipulation using dual arms equipped with the developed hands.

REFERENCES

[1] Jacobsen, S.C., Iversen, E.K., Knutti, D.F., Johnson, R.T., and Biggers, K.B., "Design of the UTAH/MIT dextrous hand," IEEE Int. Conf. on Robotics and Automation, pp. 1520–1532, 1986.

[2] L. B. Bridgwater, C. A. Ihrke, M. A. Diftler, M. E. Abdallah, N. A. Radford and J. M. Rogers, "The Robonaut 2 Hand ± Designed To Do Work With Tools," IEEE Int. Conf. on Robotics and Automation, pp. 3425–3430, 2012.

[3] Heni Ben Amor, Oliver Kroemer, Ulrich Hillenbrand, Gerhard Neumann, and Jan Peters, "Generalization of Human Grasping for Multi-Fingered Robot Hands," IEEE Int. Conf. on Intelligent Robots and Systems, pp.2043-2050, 2012.

[4] Kawasaki, H., Komatsu, T., and Uchiyama, K., "Dexterous anthropomorphic robot hand with distributed tactile sensor: Gifu hand II," IEEE/ASME Transactions on Mechatronics, Vol. 7, No. 3, pp. 296-303, 2002.

[5] Kaneko, K., Harada, K., and Kanehiro, F., "Development of Multi-fingered Hand for Life-size Humanoid Robots," IEEE Int. Conf. on Robotics and Automation, pp. 913 – 920, 2007.

[6] Krut, S., "A Force-Isotropic Underactuated Finger," IEEE Int. Conf. on Robotics and Automation, pp 2314 – 2319, 2005.

[7] Daniel Aukes, Susan Kimy, Pablo Garciay, Aaron Edsinger, and Mark R. Cutkosky, "Selectively Compliant Underactuated Hand for Mobile Manipulation," IEEE Int. Conf. on Robotics and Automation, pp. 2825–2829, 2012.

[8] Lael U. Odhner, Chad Walker, and Aaron M. Dollar, "Simplifying Robot Hands using Recursively Scaled Power Grasps," IEEE Int. Conf. on Intelligent Robots and Systems, pp.2910-2914, 2012.

[9] Bokman Lim, Minhyung Lee, Joohyung Kim, Jusuk Lee, Jaeho Park, Keehong Seo, and Kyungshik Roh, "Control Design to Achieve Dynamic Walking on a Bipedal Robot with Compliance," IEEE Int. Conf. on Robotics and Automation, pp. 79–84, 2012.

[10] Joohyung Kim, Younbaek Lee, Sunggu Kwon, Keehong Seo, HoSeong Kwak, Heekuk Lee, Kyungsik Roh, "Development of the lower limbs for a humanoid robot," IEEE Int. Conf. on Intelligent Robots and Systems, pp.4000-4005, 2012.

[11] Christine L. Machenzie and Thea Iberall, *The Grasping Hand*, Noth-Halland Press , pp26, 2005.

[12] Lynette A. Jone and Susan J. Lederman, *Human Hand Function*, Oxford University Press , pp12, 2006.

[13] Mahvash, M., Okamura, A., "Friction Compensation for Enhancing Transparency of a Teleoperator With Compliant Transmission", IEEE Trans. on Robotics, 2007.